DESIGN OF A DISTRIBUTED SWITCHED RELUCTANCE MOTOR FOR A TIP-DRIVEN FAN

Qiong Li[1*] – Shuirong Liao[1]

[1]College of Mechanical Engineering and Automation, Qiong Li, Huaqiao University, Xiamen, Fujian, China, 361021

Abstract:

This paper presents a design of a distributed switched reluctance motor for an integrated motor-fan system. Unlike a conventional compact motor structure, the rotor is distributed into the ends of the impeller blades. This distributed structure of motor makes more space for airflow to pass through so that the system efficiency is highly improved. Simultaneously, the distributed structure gives the motor a higher torque, better efficiency and heat dissipation. The paper first gives an initial design of a switched reluctance motor based on system structure constraints and output equations, then it predicts the machine performance and determines phase current and winding turns based on equivalent magnetic circuit analysis; finally it validates and refines the analytical design with 3D transient finite element analysis. It is found that the analytical performance prediction agrees well with finite element analysis results except for the weakness on core losses estimation. The results of the design shows that the distributed switched reluctance motor can produce a large torque of pretty high efficiency at specified speeds.

1 Introduction

Motor-fan systems are typical energy-consuming products used widely for commercial or residential equipments to ventilate air so as to transfer heat between the equipment and the environment. According to the statistical data of American Council for an Energy-Efficient Economy (ACEEE), the energy consumption of motor-fan systems is 14% of all the energy consumption of motor drive system [1]. As the growing global crisis in energy, high efficiency becomes one of the most important characteristics for motor-fan systems. To improve system efficiency, this paper presents a new motor-fan system with its motor design procedure.

Motor plays a critical role in determining fan efficiency. A properly selected and designed motor can improve system efficiency in the following way:
i. by improving efficiency itself through properly design because the higher the motor's efficiency, the higher the system efficiency;
ii. by ensuring how the fan works at a specified speed for highest efficiency since fan efficiency varies with speeds;
iii. by improving system structure to reduce air flow resistance.
SRM is a motor of high efficiency, adjustable velocity and flexible structure which has great potential for improving motor-fan system efficiency [2-6]. Although there are other motors such as ac

---

* Corresponding author. Tel.: 18906038055;
E-mail address: qiongli@hqu.edu.cn

variable frequency motor and dc motors [7-9] that can also provide unlimited specified speed, SRM is a motor type simultaneously enhancing all other properties like high efficiency, flexible structure and low cost that are required for motor-fan systems.

For a traditional motor fan assembly, the motor is often located at the center of the axis, as illustrated in Fig.1 (a) The drawback of this kind of structure is that the motor offers resistance to airflow across the blade surface so as to cut down the flow rate and system efficiency. To reduce the airflow resistance, the motor is generally compactly designed. However, the more compact the motor, the smaller the torque and power. What is more, the compact structure impedes the heat dissipation and then reduces the life expectancy of a motor.

The optimal configuration is tip-driven motor fans with motor located along the tip of the fan blade, which is presented in [10]. The new system makes more space for airflow to pass through so that the efficiency is highly improved. The researchers claim that the system efficiency can not only be twice as much the traditional system and reduce noise but larger torque can be achieved as well. Simple and flexible structures for the motor are required for the

above system. Tsai [11] designed and analyzed a computer cooling system that the brushless DC motor is distributed along the tip of fan blades. The analysis shows that the brushless motor located in this way has a considerable potential in efficiency improvement compared to a traditional motor. However, the DC brushless motor contains permanent magnet which makes the system overpriced and expansive. So, to limit its application in a motor-fan system which requires high efficiency, large output power and low cost, it should not be designed to be sensitive to accuracy velocity control.

This paper presents a new motor-fan system: a tip-driven switched reluctance motor-fan system. The presented system is based on design configuration presented in [10], as illustrated in Fig. 1(b,c). The rotor elements are embedded within the rotor ring, which forms the outer rim of the propeller fan circumference. There is no motor shaft necessary for mounting the fan and motor together. The outer rim of the propeller will be supported by 4 guide rollers (RG) located at 90 degrees apart. The rollers are fixed to the stators which are fixed to the roof of the cooling or ventilation system.
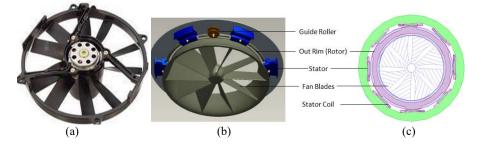

(a)   (b)   (c)

Figure 1. Structure of fan motors: (a) Traditional; (b) Prototype and (c) cross section of new distributed

The advantages for the system are as follows:
i. the distributed structure makes the air flow pass the system smoothly so as to improve the system efficiency;
ii. Switched reluctance motor can achieve pretty high efficiency;
iii. The characteristic feature of adjustable velocity for SRM enables the fan to work at specified speeds for its highest efficiency;
iv. large torque is available due to the large size of the rotor diameter;
v. SRM has a low cost construction.

This paper is mainly focused on the design of a distributed SRM for achieving desired performance under the structure constraints. The initial geometry

design uses conventional output equations [12, 13]. Unlike ordinary SRM design that the diameter of rotor is determined according to its output performance and the recommended ratio between thickness and diameter, the rotor diameter for the distributed SRM is already determined by fan diameter. Then other dimensions such as pole width, back iron thickness etc. can be decided immediately except axial length which is determined according to the desired torque value. Also, performance prediction methods based on equivalent circuit analysis are described and programs for implementing performance prediction are generated. Then the relationship curves between performance vs. phase current and winding turns are built to

determine excitation currents and turns per phase. Since the analytical methods approximate the magnetic field by representing it with several flux paths and performs 2D steady-state analysis, a finite element method is necessary to validate and refine the design. The finite element method simulates the field by dividing it into small enough elements and conducts 3D transient analysis since it is more close to practical situation and supposed to provide more accurate results.

The presented paper contains the following contents: In section 2, the analytical design process for determining geometry, phase current and winding turns is described; section 3 discusses the FEA methods for verifying and improving the motor performance; The comparison between analytical and FEA design methods as well as other considerations for a distributed SRM design are discussed in section 4. Finally, Section 5 closes the paper with brief conclusions.

2 Analytical design

2.1 Design specifications

Due to the structure of the integrated motor fan system, the output power, inner diameter and speed for the switched reluctance motor (SRM) are evaluated from fan design. This paper designs a distributed SRM to drive the fan for a commercial air cooling system. The fan is designed to remove the air flow of 3.89 m^3/s (8250 cfm) with the static pressure of 99.5 Pa (0.4 in H$_2$O). The best fan diameter of 0.72 m at the speeds of 115.2 rad/s (1100 rpm), evaluated from fan design based on Cordier diagram [14], is decided to obtain highest fan efficiency at this point. The speed, output torque, inner diameter D_{in} (as shown in Fig. 2) and other specifications for motor design are listed in Table 1.

Table 1. Specifications of the SRM

Speed	ω_{m}=115.2 rad/s
efficiency	$\eta \geqslant 0.8$
Electrical steel material property (stator and rotor)	M43: B-H & B-P characteristic [15] Chosen saturated flux density: B=1.4T Conductivity 2e6 s/m
Output torque	T=7.0 Nm
Rotor inner diameter	D_{in} =0.72 m

2.2 Geometry design

Since a SRM design involves many unknown parameters, generally it is necessary to give some insights into the remaining parameters. The given and to be determined parameters in this paper are illustrated in Fig. 2 and Table 2. Note that the rotor inner diameter D_{in} is already given in Table 1.

Given Parameters: N_s , N_r, D_{in}, β_s, β_r, l_g. q
Parameters to be determined: D, L, b_{ry}, b_{sy} , h_r,

Figure 2. Parameters for SRM design

Table 2. Given parameters for SRM design

Stator poles number	N_s =8
Stator pole angle	β_s=18^0 (0.314rad)
Air gap length	l_g=0.001m
Rotor poles number	N_r=6
Rotor pole angle	B_r=22^0 (0.384rad)
Phase	q=4

Step 1. Calculation of bore diameter D, rotor back iron thickness b_{ry}, stator back iron thickness b_{sy}, rotor pole height h_r and stator pole height h_s.

For ordinary SRM, D is determined from the output equation. In this case, D is mainly determined from the specified dimension of rotor inner diameter D_{in}, as shown in Fig. 2:

$$D = D_{in}+2h_r+2b_{ry} \tag{1}$$

where h$_r$ is estimated from the gap length l$_g$:

$$h_r \geq 20l_g \tag{2}$$

since l_g is 0.001m , then the minimum value for h_r is obtained as 0.02m.

b_{sy}, b_{ry} are calculated based on the width of the stator pole w_{sp}:

$$\omega_{sp} \geqslant b_{sy} \geqslant \omega_{sp}/2 \qquad (3)$$
$$0.75\omega_{sp} \geqslant b_{ry} \geqslant \omega_{sp}/2 \qquad (4)$$

w_{sp} is expressed as

$$\omega_{sp} = D \sin(\beta_s/2) \qquad (5)$$

To make the SRM size as small as possible, we take the minimum value for b_{ry} and b_{sy}. I.e., let b_{sy} and b_{ry} be equal to $w_{sp}/2$. As we have D_{in}=0.72m, β_s=0.314 rad. substituting (3)-(5) into (1), D is assigned to be 0.92m , w_{sp} is found to be 0.144m, and finally both b_{ry} and b_{sy} are set to be 0.08m. The stator pole height, h_s is generally decided by the number of winding turns and the size of winding. As for the initial design, assume h_r to be 0.04m.

Step 2. Estimation of the axial length L. L is determined based on output equations:

$$P_d = \eta\, k_d\, k_1\, k_2\, B\, A_S\, D^2\, L\, N_r \qquad (6)$$
$$k_1 = \pi^2/120 \qquad (7)$$
$$k_2 = 1 - 1/\sigma_s\sigma_u \qquad (8)$$

where k_d is duty cycle, A_s is specific electrical loading, σ_s is the ratio between aligned and unaligned inductance at saturation, σ_u is the ratio between aligned unsaturated inductance and unaligned inductance. They can be determined only if the machine is completely designed. As for the initial design, assume η=0.8, k_d=1, k_2=0.7, A_s=2000. Since we already have D=0.92 m, B=1.4, ω_m=115.2 rad/s, p_d=794w, T=6.9Nm, L is thus assigned to be 0.007m. So far, initial geometry design has been completed and the results are listed in Table 3. The initial geometry dimensions will be refined later if saturation happens when the desired torque is achieved.

Table 3. Results of initial geometry design

Bore diameter	$D = 0{,}92$ m
Stator back iron	$b_{sy} = 0{,}08$ m
Rotor back iron	$b_{ry} = 0{,}08$ m
axial length	$L = 0{,}007$ m
Stator pole height	$h_s = 0{,}04$ m
Rotor pole height	$h_r = 0{,}02$ m
Width of stator pole	$w_{sp} = 0{,}144$ m

2.3 Estimation of Winding Turns

The ampere turns ($T_{ph}I_P$) to produce the desired magnetomotive force (mmf) can be approximated as:

$$T_{ph}\, I_P \approx H_g * 2\, l_g \qquad (9)$$

H_g is the magnetic field intensity at air gap. When saturation begins,

$$H_g = B_{max}/\mu_0 \qquad (10)$$

in (10), B_{max} is 1.4 T, μ_0 is $4\pi*10^{-7}$, l_g is 0.001m, then H_g should be about 1114084.6 A/m and the ampere turns should be about 2400A.

For a peak phase current of $I_P = 6$ A, the number of turns per phase is

$$T_{ph}= H_g * 2l_g/I_p \qquad (11)$$

T_{ph} is found to be 400 turns per phase.
The DC supply voltage V_s can be estimated by the method presented in [13]:

$$V_s = q\, N_r\, w_m\, w_{sp}\, L\, B\, N_{Ph}/2\pi \qquad (12)$$

Since we have $q = 4$, $N_r = 6$, ω_m=115.2 rad/s, $w_{sp} = $ 0.144 m, $L = 0.007$ m, $B = 1.4$ T, $T_{ph} = 400$, then Vs is obtained as 250 V.

2.4 Evaluation of stator coil dimensions and filling factor

Assuming a current density of $J = 5$ A/mm², the area of the conductor is calculated as:

$$a_c = I_P / J\sqrt{q} \qquad (13)$$

Since $q = 4$ and $I_P = 6$ A, a_c is assigned to be 0.6 mm². The closest wire size for this cross-sectional area of the conductor is AWG #18. It has an area of 0,8107 mm² and is selected for the phase windings.
The width of the stator slot is given by:

$$w_{ss} = (\pi\, D - N_s\, w_{sp}) / N_s \qquad (14)$$

Since $D = 0.92$ m, $w_{sp} = 0.144$ m, and N_s =8, w_{ss} is assigned to be 0.217 m.
Assuming the width of the stator wedges $w = 3$ mm and packing factor $P_f = 0.8$, the number of vertical layers of winding and the number of horizontal layers of winding are obtained as:

$$N_v = P_f \cdot (h_s - w)/d_c \qquad (15)$$

where d_c is the diameter of the conductor and it is 0.813mm for AWG 20. Since h_s is 40 mm, N_v is found

to be 36.

$$N_h = T_{ph} / 2 N_v \qquad (16)$$

Since T_{ph} is 400 turns per phase and N_v is 36, then N_h is about 6.
The winding area is given by:

$$a_w = 2 \cdot a_c \, N_V \, N_h / p_f \qquad (17)$$

Since we have $a_c = 0.8107$ mm, $N_v = 36$, $N_h = 6$, $P_f = 0.8$, then a_w is obtained as 440 mm^2.
the fill factor is calculated as:

$$F_f = \frac{\text{Stator winding area}}{\text{Stator slot window area}} = \frac{a_w}{(h_s - w)w_{ss}} \qquad (18)$$

As we have $w_{ss} = 217$mm, $h_s = 40$mm, w = 3 mm, F_f is assigned to be 0.054.

2.5 Performance prediction approach

SRM performance characteristics such as efficiency, torque and output power can be estimated by establishing the relationship between flux linkages vs. current at both aligned and unaligned positions. The performance prediction approach in this paper is extracted from the 2D steady-state performance derivation method developed in [16] (refer to Appendix A for flux density evaluation and Appendix B for inductance and flux linkage calculation, respectively).
By using the above approach for flux linkage evaluation, the aligned and unaligned flux linkages of a SRM can be evaluated. Figure 3 shows the magnetization curve for the initial designed SRM.
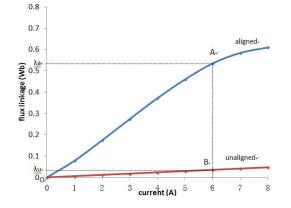

Figure 3. Magnetization curve for the initial designed SRM

As illustrated in Fig. 3, for the peak value of phase current I_p =6A, the work per stroke δW_m is the area OABO enclosed by the flux linkage curves and the vertical line of current equal to I_p:

$$\delta W_m = \text{Area (OABO)}$$
$$= \nabla i \left(\lambda_1 + \lambda_2 + \ldots + \tfrac{1}{2}\lambda_a \right) - \tfrac{1}{2}\lambda_u * I_P \qquad (19)$$

$(\lambda_1, \lambda_2, \ldots \lambda_a)$ are aligned flux linkage for phase current of (1A, 2A,...I_p); Δi, the current increment, is 1A. λ_u is the unaligned flux linkage for I_p. For this case, values for $(\lambda_1, \lambda_2, \ldots \lambda_a)$ are (0.078 wb, 0.175 wb, 0.274 wb, 0.372wb, 0.460 wb, and 0.535 wb, respectively) and λ_u is 0.02 wb, and then δW_m is obtained as 1.59J.
The average torque is

$$T_{av} = \delta W_m \, q \, N_r / 2\pi \qquad (20)$$

since $q = 4$, $N_r = 6$, T_{av} is obtained as 6,08 Nm, which is lower than the desired torque of 7,0 Nm. The output power rate is expressed as:

$$P_{out} = T_{av} \cdot \omega_m \qquad (21)$$

The efficiency is the ratio between output power and input power, which is composed of output power P_{out}, copper loss, core loss and stranded loss.

$$\eta = p_{out}/p_{in} = p_{out}/\left(p_{out} + p_c + p_s + p_{cu}\right) \qquad (22)$$

P_c is core loss estimated by using B-P characteristic of M43 and by employing the flux linkage at aligned position. P_s is stranded loss which is computed as 5% of P_{out}. Copper loss is calculated as:

$$p_{cu} = I_P^2 R_s \qquad (23)$$

R_s is the resistance of phase winding:

$$R_s = r \, l_{ph} = r \, l_{turn} T_{ph} = 2 \, r \, T_{ph} \, (D \beta_s / 2 + L) \qquad (24)$$

In addition, r is the resistivity and it is 0.021 o/m for AWG18. L_{ph} is the length of coil per phase and l_{turn} is coil length per turn.

2.6 Program for performance prediction

Excel programs (Macros) are developed in Excel VBA (Visual Basic for Applications) to implement the analytical performance prediction approach in

section 2.5. With macros, the performance characteristics including inductance, flux linkage, flux density, torque, out power, power losses and efficiency can be predicted immediately, given the information of pole number, pole arc, pole height and back iron thickness for both stator and rotor, bore diameter, stack length, air gap length as well as material properties and excitation current and winding turns. Moreover, with the help of the macros, it is convenient to adjust the design parameters to achieve desired performance.

2.7 Performance prediction for design improvement

As derived in Section 2.5, the average torque prediction for the initial design is only 6.08 Nm, which is lower than the desired torque. Then the initial design should be improved to obtain a higher torque. In this section, the factor which is to determine the torque is discussed first, and then the performance curves between efficiency and torque vs. excitation current for various turns per phase are established. The winding turns are adjusted based on the curves for desired torque and efficiency.

Step A. Performance prediction for SRM with constant ampere turns
Performance prediction for initial designed motors with the same geometry and ampere turns but various phase currents is illustrated in Table 4. It can be seen that for a SRM of determined geometry and material properties, we obtain
  i. the same ampere turns, the same flux density, torque, output power, core loss and stray loss;
  ii. The higher the phase current, the higher the copper loss and the lower the efficiency;

Step B. Establishment of the performance curves
To observe the influence of peak phase current and winding turns on motor performance, parametric analysis is performed using macros in Excel (mentioned in Section 2.6) for establishing the relationship between performance characteristic vs. excitation current and turns per phase. Table 4 shows that when peak phase current is above 8A, the efficiency is far below 0.8. To obtain design efficiency above 0.8, let the peak phase current vary from 4A to 8A (2A per step); turns vary from 360A to 660A (60 per step), the performance for 18 design points is obtained as shown in Table 5. To visually display the results in Table 5, the performance curves for average torque and efficiency vs. peak phase

current and turns per phase are established, as illustrated in Fig.4. It shows that: 1) for a desired torque, the higher the peak phase current, the less the turns per phase; 2) the efficiency is mainly affected by turns per phase. For certain peak phase current, the lower the turns per phase, the lower the efficiency. Then the same conclusion in step A can be drawn: for desired torque, the higher the peak phase current, the lower the turns per phase and the lower the efficiency.

Step C. Adjustment for winding turns
The design points for desired performance can be estimated easily from Fig. 4 and the conclusions are drawn from Table 4. For example, Fig. 4 (a) shows that the torque for the following design point is close to the desired torque of 7.0: (4A, 660), (5A, 540), (6A, 420), (7A, 360) and (8A, 360). Fig. 4 (b) shows that efficiency is close or higher than 0.8 for (4A, 660), (5A, 540), (6A, 420); lower than 0.8 for (7A, 360) and (8A, 360). So, (4A, 660), (5A, 540), (6A, 420) are acceptable design points. Namely, the points of phase current between 4 A and 6A and ampere turns of about 2520 A are close to desired points.
Exact design points for desired performance can be determined by using linear interpolation methods. For example, Table 5 shows that for I_P is 6 A, the torque is 6.3 Nm for T_{ph} of 420; 8 Nm for T_{ph} of 480. Then the torque is found to be 7.0 Nm for T_{ph} of 446, i.e., the ampere turns should be around 2680 A for a desired torque. Table 6 shows several examples of design points that can produce desired performance letting i vary from 4A to 6A, 1A per step. From overall tendency and the examples, it can be seen that the design points with ampere turns equal or very close to 2680 and phase current no more than 6A can produce desired performance of torque and efficiency.

2.8 Saturation check

Initial geometry design should be modified if the maximum flux density is far lower or higher than the saturated flux density. Since the diameter of the SRM in the presented system is mainly controlled by fan size, the axial length is the main dimension to be modified if necessary.
Motor geometry dimensions do not need to be modified because: 1) the B_s in Table 6 just slightly exceeds the saturated flux density; 2) the B_s is an approximate value obtained by using both simplified magnetic circuit analysis and other assumptions. Decision for geometry modification will be made later considering FEA validation results.

Table 4. Analytical performance prediction for initial design

No	I_p (A)	T_{ph}	$T_{ph} I_p$ (A)	B_s (T)	T_{av} (Nm)	P_{out} (W)	P_{cu} (W)	P_c (W)	P_s (W)	η
1	4	600	2400	1.32	6.08	700.6	61.1	61.2	34.9	0.816
2	6	400	2400	1.32	6.08	700.6	91.6	61.2	35.0	0.789
3	8	300	2400	1.32	6.08	700.6	122	61.2	35.0	0.762
4	10	240	2400	1.32	6.08	700.6	153	61.2	35.0	0.738
5	12	200	2400	1.32	6.08	700.6	183	61.2	35.0	0.715

Table 5. Results for parametric analytical analysis.

No	I_p (A)	T_{ph}	T_{av} (Nm)	B_s (T)	P_{out} (W)	P_{cu} (W)	P_c (W)	P_s (W)	η
1	4	360	2	0.83	229	36.7	25	11.4	0.757
2	6	360	4.6	1.22	530	82.4	50.5	26.5	0.768
3	8	360	8	1.46	927	147	76.2	46.4	0.774
4	4	420	2.8	0.97	317	42.7	33	15	0.775
5	6	420	6.3	1.39	721	96.2	67	36	0.782
6	8	420	10.5	1.53	1214	171	87.3	60.7	0.791
7	4	480	3.6	1.09	417	48.8	41.5	20.9	0.788
8	6	480	8	1.46	923	110	76.2	46.1	0.798
9	8	480	13	1.58	1504	195	96.7	75.2	0.803
10	4	540	4.6	1.22	530	55	50.5	26.5	0.8
11	6	540	9.9	1.51	1137	124	84.6	56.9	0.81
12	8	540	15.7	1.63	1805	220	104	90.2	0.813
13	4	600	5.7	1.32	652.5	61.1	60	32.6	0.808
14	6	600	11.75	1.55	1354	137	92.2	67.7	0.819
15	8	600	18.3	1.66	2106	244	109.3	105.3	0.82
16	4	660	6.8	1.41	784	67.2	70.3	39.2	0.815
17	6	660	13.7	1.59	1578	151	98.7	78.9	0.827
18	8	660	20.96	1.7	2415	269	113.4	120.8	0.827

Figure 4. Relationship curves between (a) torque and (b) efficiency vs. excitation current for various turns per phase.

3 FEA validation

3.1 Finite element modeling

3D transient Finite element analysis employing electromagnetic field simulation software (ANSYS Maxwell) is conducted for simulating the SRM magnetic field. A SRMCore generation application of the software is applied to create rotors and stators geometry automatically. Models of initial designed SRM are generated as shown in Fig. 5(a). Mesh for the SRM are illustrated in Fig. 5 (b). For

simplicity, ideal current wave designed based on ideal inductance profile is assigned for excitation. Figure 6 shows the shape of the idea inductance profile and current wave for the SRM during a period.

3.2 FEA validation for analytical design

Table 7 shows the FEA performance prediction for the design in Table 6. The FEA results are pretty close to analytical results except that:

i. Current loss, which is a component of core loss and too complicated to be calculated by analytical methods, is obtainable by FEA;

ii. B_s is slightly lower than that of analytical prediction. Hence, T, P_{out}, P_c P_s are slightly lower than analytical prediction;

iii. Efficiency is close and slightly higher than that of analytical prediction.

3.3 Establish of FEA performance curves

To validate analytical prediction and refine the design, parametric FEA are performed. Design points for parametric FEA are the same as those for analytical parametric analysis shown in Table 5. Then, the FEA results for 18 design points are obtained as listed in Table 8. The performance curve of torque and efficiency is shown in Fig. 7, which shows the same performance tendency as that of Fig. 4: for a desired torque, the higher the phase current, the less the turns per phase, the lower the efficiency.

3.4 FEA design refinement

The points that produce torque close to the desired value are (4A, 670), (5, 540), (6, 480), (7, 420), (8, 360), as illustrated in Fig. 7(a). Fig. 7(b) shows that efficiency is above 0.8 for design points of (4A, 670), (5, 540), (6, 480) and lower than 0.8 for the points of (7, 420), (8, 360). It can be seen that for desired torque and efficiency, the phase current should be no more than 6A.

From Table 8 or Fig. 7 (a) it can be seen that the torque is 5.9Nm when i is 6 and T_{ph} is 420; 7.6Nm when i is 6 and T_{ph} is 480. By using interpolation method, it can be derived that the torque is 7.0 when i is 6 and T_{ph} is 460, i.e., ampere turns should be around 2760 for a torque of 7.0Nm. Table 9. shows the performance obtained by FEA letting i vary from 4A to 6A, 1A per step; $T_{ph}i$ remain 2760A. It shows that when i is equal to 6A, the efficiency is equal to 0.8. Then considering the performance tendency described in section 3.3, it can be concluded that the desired torque and efficiency can be obtained when $T_{ph}i$ is 2760 A and phase current is no more than 6A.

3.5 Detailed FEA performance prediction for a desired design.

Now, the final design is obtained with peak phase current of 6A, winding turns of 460 and geometry dimensions shown in Table 2 &3. The supply voltage should be modified from 250 V to 280 V following the method in section 2.3. The filling factor will be modified from 0.054 to 0.063 following the method in Section 2.4.
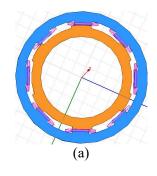
To find desired design, the previous parametric FEA only focuses on the performance of average torque and efficiency vs. phase current and turns per phase. FEA is performed in order to observe the performance in detail for the final design. Performance curves of torque and efficiency vs. time, as illustrated in Fig. 8 (a-b), show that the average torque is 7.0 Nm and the efficiency is 0.798. Output power vs. speeds is shown in Fig. 8 (c). It can be seen that the SRM has the highest output power at the specified speeds of 115.2 rad/s. Fig. 8(d) shows the flux density distribution of the SRM. It is found that the maximum value of B_s is about 1.37 T, which means that no saturation happens for this design. FEA results in Fig. 8 show that the preliminary design meets system design requirements.

Table 6. Examples of analytical design points that can produce desired performance.

No	I_p (A)	T_{ph}	$T_{ph}I_p$ (A)	B_s (T)	T_{av} (Nm)	P_{out} (W)	P_{cu} (W)	P_c (W)	P_s (W)	η
1	4	670	2680	1.42	7.0	806.7	68.2	72.7	40.3	0.817
2	5	536	2680	1.42	7.0	806.7	85.2	70.1	40.3	0.803
3	6	446	2676	1.42	7.0	804.3	102.	72.6	40.3	0.796

Table 7. FEA Performance prediction for the variations in Table 6.

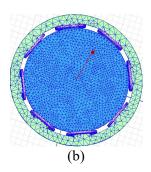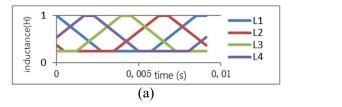| NO	I_p (A)	T_{ph}	$T_{ph} I_p$ (A)	B_s (T)	T (Nm)	P_{out} (w)	P_{cu} (W)	P_c (W)		P_s (W)	η
								Hysteresis	current		
1	4	670	2680	1.35	6.64	765.0	80.2	56.2	48.4	38.8	0.83
2	5	536	2680	1.35	6.64	765.3	100.2	56.2	48.4	38.8	0.81
3	6	446	2672	1.34	6.62	763.0	135.4	56.1	48.3	38.7	0.80

(a) (b)

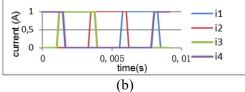*Figure 5. FEA models for (a) geometry (b) mesh*

(a) (b)

Figure 6. Ideal profile for (a) inductance; (b) current of designed SRM

Table 8. The results of parametric FEA

No	I_p (A)	T_{ph}	B_s (T)	T_{av} (Nm)	P_{out} (W)	P_{cu} (W)	P_c (W)		P_s (W)	η
							Hysteresis	current		
1	4A	360	0.85	2.0	234.3	43.0	29.0	20.4	11.1	0.75
2	6A	360	1.2	4.5	513.2	97.0	46.1	37.1	25.4	0.76
3	8A	360	1.4	7.6	870.5	172.4	59.2	53.4	44.8	0.77
4	4A	420	1.0	2.7	316.8	50.3	35.2	26.1	15.2	0.77
5	6A	420	1.3	5.9	683.8	113.1	53.6	44.6	34.3	0.79
6	8A	420	1.5	9.9	1139.2	201.1	65.5	65.5	61.0	0.79
7	4A	480	1.1	3.6	410.2	57.5	41.3	31.3	19.9	0.79
8	6A	480	1.4	7.6	870.5	129.3	59.2	53.4	44.8	0.80
9	8A	480	1.6	12.4	1425.5	229.8	71.0	76.9	79.7	0.81
10	4A	540	1.2	4.5	513.2	64.6	46.8	36.4	25.2	0.81
11	6A	540	1.5	9.3	1070.2	145.4	64.0	62.5	56.7	0.82
12	8A	540	1.7	15	1726.2	258.5	75.9	86.6	100.8	0.82
13	4A	600	1.3	5.4	625.0	71.8	51.5	41.8	31.1	0.82
14	6A	600	1.6	11.1	1280.4	161.6	68.4	71.4	70.0	0.83
15	8A	600	1.8	17.7	2039.8	287.3	80.3	94.7	124.4	0.83
16	4A	660	1.4	6.5	744.4	79.0	55.5	47.4	37.6	0.83
17	6A	660	1.7	13	1499.4	177.7	72.3	79.5	84.7	0.84
18	8A	660	1.8	20.5	2365.5	316.0	84.2	101.5	150.6	0.84

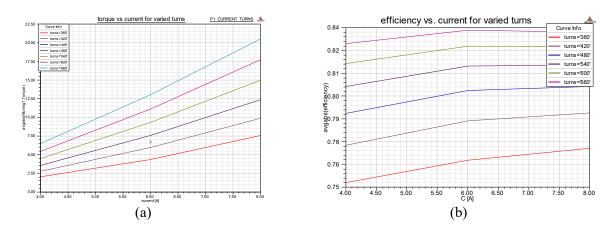(a)   (b)

Figure 7. FEA results for (a) torque (b) efficiency vs. phase current for varied winding turns per phase

Table 9. FEA design results (L=0.007)

No	I_p (A)	T_{ph}	$T_{ph} I_p$ (A)	B_s (T)	T (Nm)	P_{out} (W)	P_{cu} (W)	P_c (W)		P_s (W)	η
								Hysteresis	current		
1	4	690	2760	1.37	7.0	806.7	82.6	57.4	50.4	41.2	0.83
2	5	552	2760	1.37	7.0	806.7	103.2	57.4	50.4	41.2	0.82
3	6	460	2760	1.37	7.0	807.0	123.9	57.4	50.4	41.2	0.80

(a)   (b)

(c)   (d)
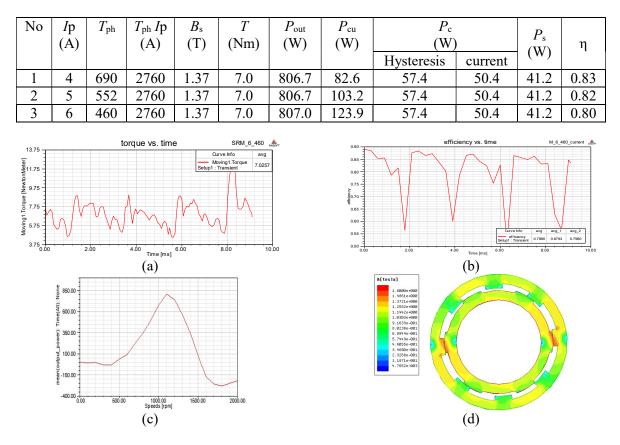
Figure 8. Characteristic features of a design: (a) torque vs. time; (b) efficiency vs. time; (c) output power vs. speeds; (d) flux density distribution at aligned position.

4   Discussion

4.1 Discussion of the analytical performance prediction

The following discussion is based on the analytical performance prediction shown in Table 4:

i. Once the geometry dimensions and material properties have been determined, the flux density (B_s) is determined by ampere turns (T_{ph} i). This tendency agrees with Ampere's Law Meanwhile, the performance of output torque, core loss and stray loss are also determined by ampere turns since they are completely decided

by flux density.

ii. As the excitation current (i) increases, the copper loss increases and the efficiency decreases. It can be explained using Eq. (23-23).

iii. The analytical evaluation of B_s and torque is lower than desired B_s (1.4T) and torque (7.0Nm). The reason is that 2400A is an approximate value for ampere turns: it is derived from the maximum mmf at the air gap (Eq. (9)). The actual mmf should be higher since it contains the mmf produced at all the segments in a flux path (Eq. (27), Appendix A). Namely, the actual torque should be larger than 6.08 Nm, which is actually the case.

4.2 Comparison between the FEA and analytical results

The FEA (finite element analyses) and their analytical results share the same overall tendency: 1) the same ampere turns (T_{ph} i), the same flux density; 2) the same flux density, the same torque, output power, core loss, stray loss etc. 3) the higher the phase current and copper loss are, the lower the efficiency is.

The main differences between the FEA and analytical results are:

i. FEA is able to calculate current loss, a component of core loss that is too complicated to be calculated with analytical methods. For this reason, the efficiency obtained by FEA is more accurate than that by an analytical method. As we know, the current loss is caused by using current loops which is induced by changing magnetic field. So, the same T_{ph} $i_{, and}$ the same flux densityyield the same current loss.

ii. Maximum B_s for FEA is about 7% lower than that obtained with analytical methods, which reduces torque and output power by 7% as well.

iii. Hysteresis loss and copper loss obtained by FEA are very close while slightly different from analytical methods.

Reasons for the above differences are:

i. The analytic method simplifies the magnetic field by representing the magnetic field with only several flux paths assuming that the flux density is distributed evenly in each path. However, the finite element method simulates the magnetic field by dividing the whole field into pretty small elements and by computing the flux density for each element. This is the main

explanation for the difference between analytical and FEA prediction of the flux density.

ii. 3D transient FEA estimates the performance at small time step during a period. The torque, losses and efficiency are the average value of corresponding results of the entire time step. Therefore, analytically obtained results agree with a steady-state analysis. The torque, losses and efficiency are roughly derived from flux linkage vs. current curves at unaligned and aligned position. It explains why, Table 7shows that the output power is lower, the losses are higher and efficiency is slightly higher than those items presented in Table 6.

iii. the FEA considers the overlap between the phases while the analytical methods ignore the overlap.

The above discussions show that the FEA simulation is closer to the practical situation and more accurate than the analytically presented results. However, the analytical results can be obtained faster than those with FEA and besides are very reliable for a qualitative analysis. The analytical performance prediction of a design point can be obtained in a second with macros while it takes dozens of minutes to obtain a FEA result. The best way for obtaining approximated design points and redesigning a particular detailed case study is to use analytical methods with the help of FEA.

4.3 Characteristics for the distributed SRM

The distributed SRM is characterized by the following:

i. Pretty high efficiency is possible since large winding turns number is allowable. Design results for desired torque show that the lower the phase current is, the larger the number of winding turns and consequently the higher efficiency. Considering the space available for coils, the number of winding turns in a conventional SRM should not be very large Consequently, a large number of winding turns, may cause the problem of heat dissipation in a compact machine structure. However, in the concept of a distributed SRM there is spacious space for coils since the bore diameter is large in size. The derivation in section 2.4 shows that the fill factor is less than 7%.

ii. High power can be obtained since the distributed structure gives no limitation for a given motor volume. High power is available

when the motor volume is large enough.

iii. Since the axial dimension of the SRM is pretty small compared to the radial dimension, it may cause problems in manufacturing or structure strength. There are several options for solving the problem:

a) more guided rollers (or other types of supports) can be added to the outer rim fan to enhance the strength in axial direction if necessary;

b) the axial length can be larger without wasting material when using the laminar steel of lower saturated flux density;

c) the axial length is to be enlarged to some extent if necessary provided that the laminar steel is at low cost in comparison with the permanent magnet.

5   Conclusion

A distributed SRM for an integrated motor-fan system is introduced and designed to meet the desired system performance requirements. Initial geometry is estimated based on structure constraints and output requirements. Excel programs (Macros) are generated for analytical performance prediction based on magnetic equivalent circuit analysis. The excitation current and winding turns are determined from the performance curves generated by using macros. The analytical design is validated and refined with the help of 3D transient FEA. The results show a good concurrence between the two methods except for core loss evaluation. The results show that the designed SRM can achieve desired torque and efficiency of 80% or even higher when working at the speeds specified by fan design. According to the tendency of performance vs. phase current and winding turns, it is found that pretty high efficiency is possible for a distributed SRM since there is spacious space for coils of large number of winding turns.

6   Acknowledgements

7   References

[1] Elliott, R. N., Nadel, S.: *Fan and pump systems: markets and programs,* American Council for an Energy-Efficient Economy, Washington, DC, 2002.

[2] Ray, W. F., Lawerson, P. J., Davis, R. M., Stephenson, J. M., Fulton, N. N., Blake, R. J.: *High performance switched reluctance brushless drives.* IEEE Trans. Ind. Appl., IA-22 (1986), 4, 722–730.

[3] Byrne, J. V., O'Dwyer, J. B., Mcmullin, M. F.: *A high performance variable reluctance drive: A new brushless servo.* Power Convers. Int. Mag., 1986, 60–66.

[4] Rahman, K. M., Fahimi, B., Suresh, G., Rajarathnam, A. V., Fhami, M.: *Advantages of switched reluctance motor applications to EV and HEV: Design and control issues,* IEEE Trans. Ind. Appl., 36 (2000), 1, 111–121.

[5] Rahman, K. M., Schulz, S. E.: *Design of high-efficiency and high-torque—density switched reluctance motor for vehicle propulsion,* IEEE Trans. Ind. Appl., 38 (2002), 6, 1500–1507.

[6] Vijayakumar, K., Karthikeyan, R., Paramasivam, S. , Arumugam, R., Srinivas, K. N.: *Switched Reluctance Motor Modeling, Design, Simulation, and Analysis: A Comprehensive Review,* IEEE Trans. Magn., 44 (2008), 12, 4605-4617.

[7] Saidur, R., Mekhilef, S., Ali, M. B., Safari, A., Mohammed, H. A.: *Applications of variable speed drive (VSD) in electrical motors energy savings,* Renew. Sust. Energ. Rev., 16 (2012), 1, 543-550.

[8] De Almeida, A.T., Ferreira, F. J. T. E., Both, D.: *Technical and economical considerations in the application of variable-speed drives with electric motor systems,* IEEE Trans. Ind. Appl., 41 (2005), 1, 188 - 199.

[9] Liu. Y., Wang. X., Xing. Y.: *An improved three-level direct torque control method of brushless doubly-fed machine based on the fixed synthesizing vector,* Engineering Review, 33 (2013), 3, 203-209.

[10] Technology news: *Tip-driven fan is twice as efficient.* Drives and Controls, 2000, http://www.drives.co.uk/fullstory.asp?id=1375.

[11] Tsai, M. C., Weng, M. H., Hsieh, M. F.: *Computer-Aided Design and Analysis of New Fan Motors.* IEEE Trans. Magn., 38 (2002), 5, 3467-3474.

[12]Krishnan, R., Arumugam, R., Lindsay, J. F.: *Design procedure for switched reluctance motors,* IEEE Trans. Ind. Appl., 24 (1988), 3, 456–461.

[13] Miller, T.J.E.: *Switched reluctance motors and their control,* Clarendon, Oxford U. K., 1993.

[14] Wright, T.: *Fluid Machinery: Performance, Analysis, and Design.* CRC press, 1999.

[15] Armco INC. *B-H and core loss data for Armco Silicon Steels.* http://www.protolam.com/page5.html.

[16] Krishnan, R.: *Switched reluctance motor drives: Modeling, simulation, analysis, design and applications.* 1st ed. CRC press, 2001.

Appendix A. Flux density evaluation

Flux density evaluation is critical for flux linkage estimation. Assuming several flux paths for each rotor position, once the flux density for each path is determined, the total inductance and flux linkage can be evaluated. The process for determining the flux density for each path is an iteration process.

Take the aligned position as an example, seven flux paths are assumed for the aligned position as illustrated in Fig. 9(a). Path 1 to 6 are identical except path 7. Establish magnetic equivalent circuit for each path. The magnetic equivalent circuit for mutual path1 and path 7 are shown in Fig. 9(b-c).

Assuming an initial value for stator pole flux density in path 1(B_{sp1}), then the flux density of all the other segment in path 1 can be determined since flux 1 in each segment is identical:

$$\Phi_1 = B_{sp1}A_{sp1} = B_{rp1}A_{rp1} = \\ = B_{sy1}A_{sy1}B_{ry1}A_{ry1} = B_{g1}A_{g1} \qquad (25)$$

B_{rp1}, B_{sy1}, B_{ry1} and B_{g1} are flux density for rotor pole, stator back iron, rotor back iron and air gap in path 1; A_{sp1}, A_{rp1}, A_{sy1}, A_{ry1} and A_{g1} are cross section area of corresponding segments for path 1.

For each circuit, the magnetomotive force (mmf) for various segment can be calculated by applying ampere's circuital law:

$$F_1 = 2\left[H_{sp1}l_{sp1} + H_{rp1}l_{rp1} + H_g l_{g1}\right] \\ + \left[H_{ry1}l_{ry1} + H_{sy1}l_{sy1}\right]/2 \qquad (26)$$

Where H_{sp1}, H_{rp1}, H_{g1}, H_{sy1}, H_{ry1} are the magnetic field intensity in each segment. For given flux density, the magnetic field intensity can be extracted from the B-H characteristic. l_{sp1}, l_{rp1}, l_{g1}, l_{sy1}, l_{ry1} are length of each segments for path 1. Expressions for describing cross section area and length for each segments of path 1 is given in [16].

The error between calculated and applied mmf ($T_{ph}i$) is:
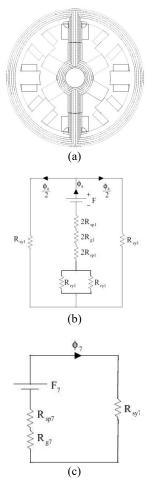
$$\Delta F = T_{ph}i - F_1 \qquad (27)$$

Figure 9. (a) Flux paths; (b) equivalent circuit for mutual path 1; (c) equivalent circuit for path 7 at aligned position [16]

The assumed flux density should be increased for a positive error or decreased for a negative error and repeat the above process until the error is reduced to an acceptable tolerance limit. In this way the final flux densities for various parts are obtained.

Appendix B. Inductance and flux linkage calculation

The inductance for flux path 1 is

$$L_{a1}=T_{ph}{}^2/(2R_{sp1}+2R_{g1}+2R_{rp1}+\frac{R_{sy1}}{2}+\frac{R_{ry1}}{2}) \qquad (28)$$

R_{sp1}, R_{rp1}, R_{g1}, R_{sy1}, R_{ry1} are reluctance for stator pole, rotor pole, air gap, stator back iron, rotor back iron respectively. They can be calculated according to the flux density evaluated in part A, the B-H characteristic and machine geometry. For example, R_{sp1} is calculated as:

$$R_{sp1}=H_{sp1}l_{sp1} / B_{sp1}A_{sp1} \qquad (29)$$

Once obtaining inductance for each path through magnetic equivalent circuit analysis, the total inductance at the aligned position is the sum of the inductances for all the seven paths:

$$L_a=\sum_{k=1}^{7} L_{ak} \qquad (30)$$

The flux linkage at the aligned position is the product of inductance and phase current:

$$\lambda_a=L_a i \qquad (31)$$

Flux linkage at unaligned position (λ_u) can be calculated with a similar procedure except different magnetic equivalent circuit for each path due to different shape of flux path, as illustrated in Fig. 10.
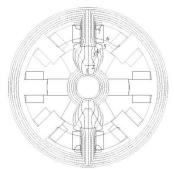

Figure 10. Flux paths for unaligned position [16]